18

Utilizing the Functional Work Space Evaluation Tool for Assessing a System Design and Reconfiguration Alternatives

A. Djuric and R. J. Urbanic
University of Windsor
Canada

1. Introduction

1.1 Problem definition

The 'boundary of space' model representing all possible positions which may be occupied by a mechanism during its normal range of motion (for all positions and orientations) is called the work envelope. In the robotic domain, it is also known as the robot operating envelope or workspace (Nof, 1999). Several researchers have investigated workspace boundaries for different degrees of freedom (DOF), joint types and kinematic structures utilizing many approaches (Ceccarelli , 1996), (Ceccarelli & Vinciguerra, 1995), (Ceccarelli & Lanni, 2004), (Cebula & Zsombor-Murray, 2006), (Castelli, et al., 2008), (Yang, et al., 2008). A recent example utilizes a reconfigurable modeling approach, where the 2D and 3D boundary workspace is created by using a method identified as the Filtering Boundary Points (FBP) algorithm. This is developed fully in Djuric and ElMaraghy (2008).

However, this work envelope based work is limited as it does not contain relevant information regarding the relationships between the robot, or mechanisms within a system. This includes the general kinematic structures within the system, the location of the working part(s), tools, process parameters and other operation related parameters. Here an operation is defined as consisting of the travel path, manipulator/end-effector or working tool, tool and part location, and orientation, and any other related process related parameters. The work envelope provides essential boundary information, which is critical for safety and layout concerns, but the work envelope information does not by itself determine the feasibility of a desired configuration. The effect of orientation is not captured as well as the coupling related to operational parameters. Included in this are spatial occupancy concerns due to linking multiple kinematic chains, which is an issue with multi-tasking machine tools, reconfigurable machines, and manufacturing cells.

Multi-tasking machine tools can be considered CNC mill-lathe hybrids (Figure 1). These machines enable multiple tool engagement in multiple parts simultaneously. Each tool/ part/ spindle/ axis set combination follows its own unique programmed path. These machines minimize the number of manual operations, as well as reduce setup costs and potential quality issues. A single multi-tasking machine tool can completely machine complex parts from start to finish (Hedrick & Urbanic, 2004). Traditional computer numerical control (CNC) machines consist of multiple kinematic chains (two – one to

support the tool and the other to support the fixture), and can be defined by standard families, i.e., 3 axis horizontal machine, 3 axis vertical, 4 axis horizontal and so forth. The valid kinematic chain loops need to be defined, but are static. It must be noted that depending on the machine type and configuration for multi-tasking machines, the kinematic chain loops can dynamically change, which is beyond the scope of this work, but needs to be considered when assessing the feasibility in time and space of these machine families.

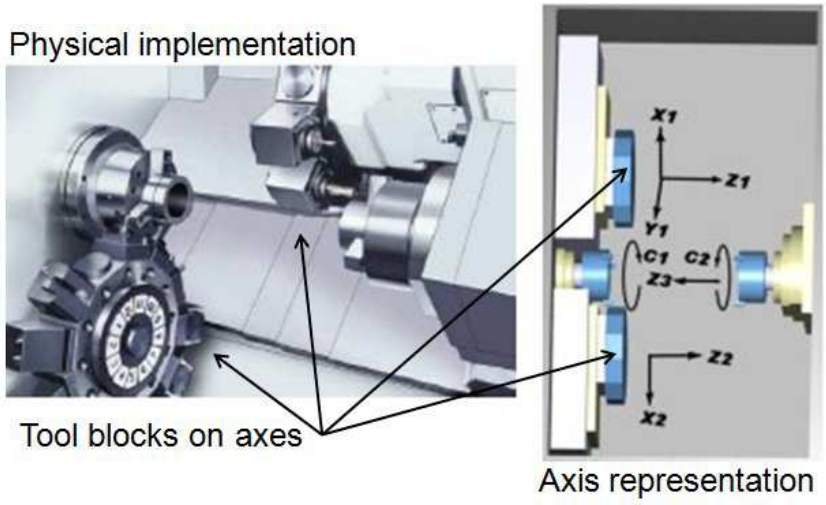

Fig. 1. Okuma LT300-MY (Okuma, 2002) and Programmable Axes (adapted from Hedrick & Urbanic, 2004)

In any manufacturing environment, responsiveness to unforeseen disturbances on the shop floor is highly desirable in order to increase throughput, reduce waste and improve resource utilization and productivity (ElMaraghy, 1993). Process improvement methods to increase shop floor responsiveness while minimizing capital investments have consistently been a topic for manufacturing research. This is presently being addressed through the concept of reconfigurable manufacturing (ElMaraghy, 2008). The key building blocks of a reconfigurable manufacturing system are scalability, adaptability, and transformability (Koren et al., 1999). This should reduce capital investments over the system life cycle, rapid changeovers, steeper launch curves, and minimal fluctuations in quality and this has great future potential (Anderson & Bunce, 2000). The reconfiguration concept is divided into two subsets for this work: extendibility (Figure 2) and reconfigurability (Figure 3).

Changing cutting tools, the tooling systems used to mount the tools into the machine, the end-effector or replacing an axis with another with different constraints is considered extendibility. For machining, this usually introduces shifts in the working boundaries allowing the same programs / travel paths to be used with appropriate offsets.

For robotic applications, this may not be the case. (Note: for systems where the end-effector requires specific orientations, it is assumed that the orientation remains constant for a given length offset.) These modifications are typically made in the tooling domain.

A reconfiguration consists of altering the machine topology, i.e. changing the DOF by adding or removing an axis. This may require re-programming, or depending on the

reconfiguration, a totally different programming or process planning strategy may be required.

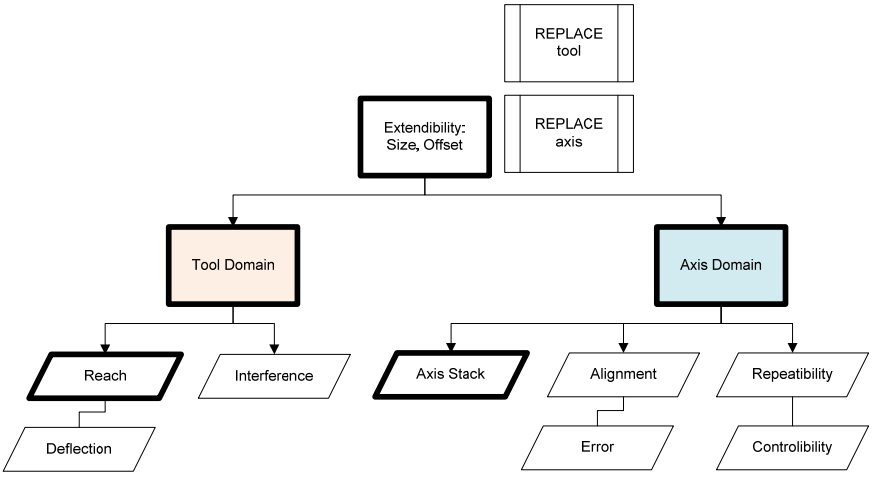

Fig. 2. Extendibility breakdown

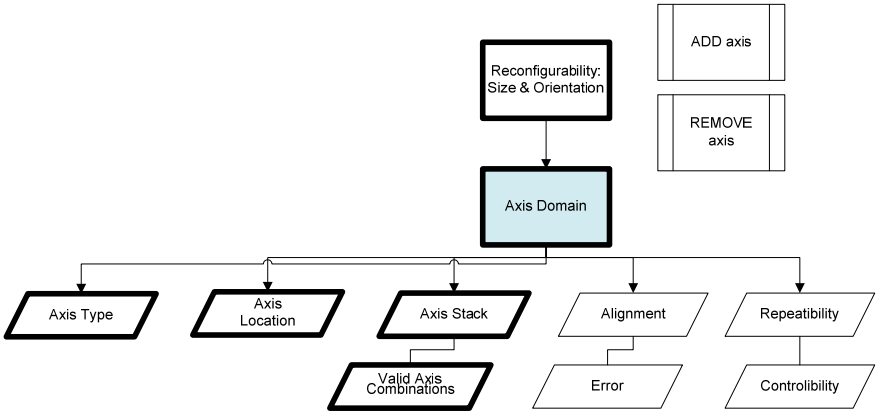

Fig. 3. Reconfigurability breakdown

The work envelope does not allow one to assess the operating feasibility of a machine, robot, or system configuration for a set of tasks. Another assessment parameter needs to be introduced to indicate the functional operating work space. Hence, the work window is introduced, and is defined as the valid functional space for a configuration to allow a kinematic structure (robot, machine tool, manufacturing cell, etc.) to follow a path for a set of conditions relating to the system configuration, tooling, fixture location and so forth (Djuric & Urbanic, 2009). A part may be located within the work envelope, but it may not be within the work window. In Figure 4, the encircled region cannot be reached for the 'normal to the base' orientation for the 6R Fanuc robot although the part is within the envelope. The items bounded by a bolded line in Figures 2 and 3 are discussed in this research.

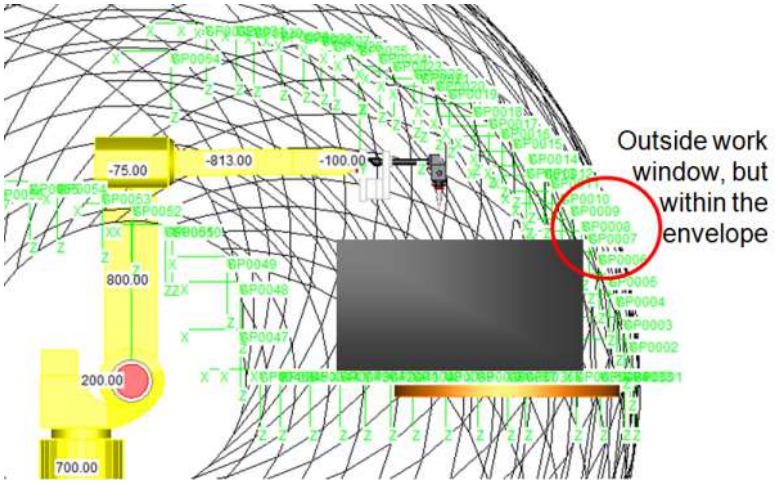

Fig. 4. Work envelope and work window for a 6R Fanuc robot (Djuric & Urbanic, 2009)

The actual work window conditions will vary based on the part, travel path tool parameters, geometry, machine kinematic composition and the application. For machining operations, the work window will vary for each unique orientation/ tooling /fixture combination. Structural reconfigurations, such as adding or removing an axis (DOF and type of joints) either virtually or physically, will also impact the work window. A methodology needs to be developed to define the work window for a configuration, and any potential reconfigurations. The assessment of system elements is necessary in order to examine the feasibility and practicality of a set of kinematic structures in a manufacturing scenario. This does not exist at this time. There is a direct relation between the kinematic structures, their manipulability and constraints, to the work window. Proper assessment of system elements will help in optimization of a system and help in deciding various parameters such as number of degrees of freedom, placement of machines, robots and other supporting mechanisms (in case of a work cell consisting of multiple kinematic chain elements) and so forth. The methodology needs to be applicable for the reconfigurable type of machinery. The goal of this work is to focus on foundational work window assessment approaches.

1.2 Research approach

This structure of the chapter is as follows. First, the assessment methodology for machine tool type mechanisms is presented. An appraisal of "primitive" or basic kinematic building blocks is performed and a breakdown of their characteristics is presented. These elemental building blocks are used to create the basic working boundaries using geometric modelling techniques and Boolean operations for more advanced kinematic structures.
A different solution approach is required for the selected industrial robot families (ABB and Fanuc), which is presented in detail in this work. However, the Boolean approach in order to couple the operating environment to the kinematic structure is common. The case study in this work in centred on a robotics work cell application. The feasibility of solution alternatives can then be assessed, as well as the determination of alternative options, which is explored in the case studies section. This research work is then summarized and concluded.

2. Methodology to define the work window

The approaches to determine the work window are different for machine tool type kinematic structures and 6 DOF robots at the base level due to their unique topologies. The machine tool type of devices is decomposed into elemental or primitive groups. The term primitive is utilized, as basic mathematical definitions are used to present the regions of interest. Combining these primitive elemental structures to characterize a selection of machine tools is then illustrated. The methodology to couple the fixture based and tooling based kinematic chains is then presented.
For the selected industrial robot families, an empirical and detailed analytical methodology to determine the workspace boundary for a desired orientation is presented, along with illustrative examples.

2.1 Decomposition analysis for machines consisting of elemental combinations

Machine types consisting of primitive elemental combinations are milling machines, lathes, routers, coordinate measuring machines (CMM's), and so forth. There are standard machine families, but there are also specialty combinations that are becoming more ubiquitous. There are several basic travel paths strategies that can be employed. The types and typical applications are as follows:

- 2 axis (X, Y) travel path motion (used for tool less profile machines such as water jet, plasma jet and laser cutting – this is trivial as the work space = work window and is a rectangular surface bounded by the axis stroke limits. This is presented as Case 4 in Table 1.)
- 2 axis (Z, X) travel path motion + rotary spindle (used for lathe machining – this is a subset of Case 4 in Table 1. The axes only move in Z and X, but are swept in a rotary profile)
- 2 axis (X, Y) + Z depth ('2 ½ axis') travel path motion (used for additive manufacturing machines – this is trivial as the work space = work window and is a surface bounded by the axis stroke limits, incremented by a specific Δz value. This is a subset of Case 6 in Table 1.)
- 3 axis travel path motion (used for standard milling machines – the work window is offset from the workspace by the length of the tool and is a solid, also bounded by the axis stroke limits. This is presented by Case 6 or Case 4 in combination with the Case 0, *T* in Table 1.)
- 3 axis travel path motion and 1 or 2 axis rotary positioning (used for standard 4 and 5 axis milling machines, and 5 axis CMMs. These are combinations of Cases 4-6 and 8-10 in Table 1.)
- 5 axis travel path motion and (used for 5 axis milling machines. These are combinations of Cases 4-6 and 8-10 in Table 1.)

More sophisticated machines, such as multi-tasking machines (Figure 1), consist of a combination of 3, 4, and 5 axis sub-machines on a lathe frame. The valid kinematic chain combinations must be understood for these machines. The common characteristic of these types of mechanisms is that they can be broken down into basic primitive elemental structures. One kinematic chain holds the tool, the other the part. These elemental structures are combined to create a closed kinematic loop. The reference planes reflect how the axes are physically stacked, and the datum locating points between these elemental structures, and

are used to link relationships to define the usable three dimensional (3D) space. It is readily evident that the work envelope essentially consists the bounding stroke positions of the linear or translational axes. The process flow for determining the work window for these mechanisms is illustrated in Figure 5.

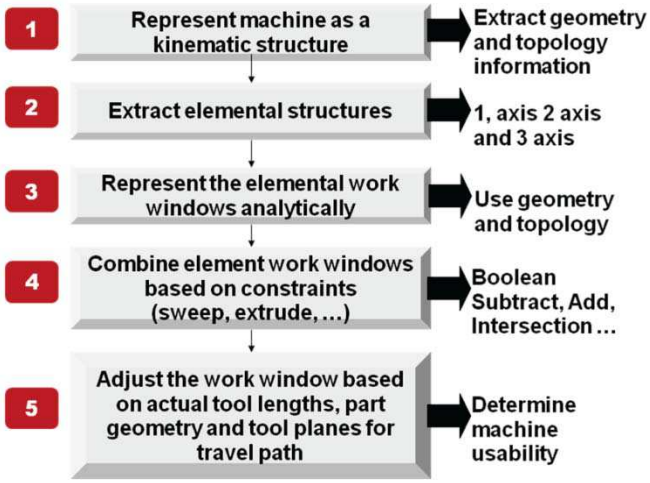

Fig. 5. Work window algorithm for mechanisms created from elemental kinematic chains, adapted from Djuric & Urbanic, 2009

To assist with steps 1 and 2 in the process flow, the workspace and window are analysed for a set of 2 and 3 DOF kinematic structures (a selected set presented in Table 1). The *R* represents a rotary axis, and the *T* a translational axis. For this work, it is assumed that axes are stacked orthogonally. The coded delineation represents the axis stack, i.e., *RT* indicates that a translational axis is orthogonally stacked at the end of a rotary axis (Case 2 in Table 1). When specific subscripts are included, for example Case 8 - $T_X R_B$, this is used to indicate an axis placed on top of another axis, in the order listed. The *A* axis rotates around the *X* translational axis, the *B* axis rotates around the *Y* translational axis, and the *C* axis rotates around the *Z* translational axis.

The workspace of the 2 DOF mechanisms may be a surface, curve or line. Depending on the axis combination and axis stack, the bounding conditions for an axis combination may be a segmented line – i.e., a void exists where the axis/part / fixture is located. The 3 DOF mechanisms usually have a solid workspace. Again, this depends of the joint type (rotational or translational) and their order in the kinematic chain. The revolve profile consists of the sweep volume of the rotary axis, part, and fixture profiles around the rotation axis.

Two combinations of vertical 3 axis milling machines are shown in Figure 6, which are comprised of Case 0, T and Case 4. In Figure 7, a 5 axis vertical milling machine which is comprised of Cases 5 and 6 is shown. In Figure 8, a horizontal 5 axis milling machine is illustrated, which is comprised of Cases 4 and 9. For this machine, the revolve profile is also displayed.

Case	Kinematic Structure	Label	Workspace	Work window	Comment
0, T		T	-	-	1 DOF basic element
0, R		R	-	-	1 DOF basic element
1		RR	Flat circular surface	Flat circular surface	Work space = Work window
2	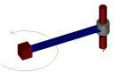	RT	Cylindrical surface	Cylindrical surface	Work window = Work space - tool length
3		TR	Cylindrical surface	Cylindrical surface	Work window = Work space - tool length
4		T_XT_Y	Rectangular surface	Rectangular Surface	Work space = Work window
5		*RR-articulated*	*Spherical surface*	*Indeterminate*	*Point position also dependent on tool length / part fixture length*
6		$T_XT_YT_Z$	Cube solid	Cube solid	Work window = Work space offset by tool length
7		*RRR-articulated*	*Toroidal surface*	*Indeterminate*	*Point position also dependent on tool length*
8	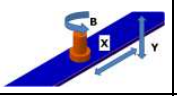	T_XR_B	**Line**	**Segmented or offset line – not completely defined until combined with other kinematic chains**	**Void in the region of the axis dependent on the revolve profile sweep radius and axis stack**
9	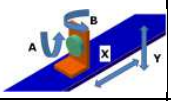	$T_XR_BR_A$	**Line**		**Void in the region of the axis dependent on the revolve profile sweep radii and axis stack**
10	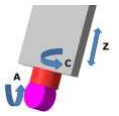	$T_ZR_CR_A$	*Hemi--spherical + cylindrical surfaces*	*Indeterminate*	**Void in the region of the axis dependent on the sweep radii and tool length**

Table 1. Summary of selected elemental structures (adapted from Djuric & Urbanic (2009)

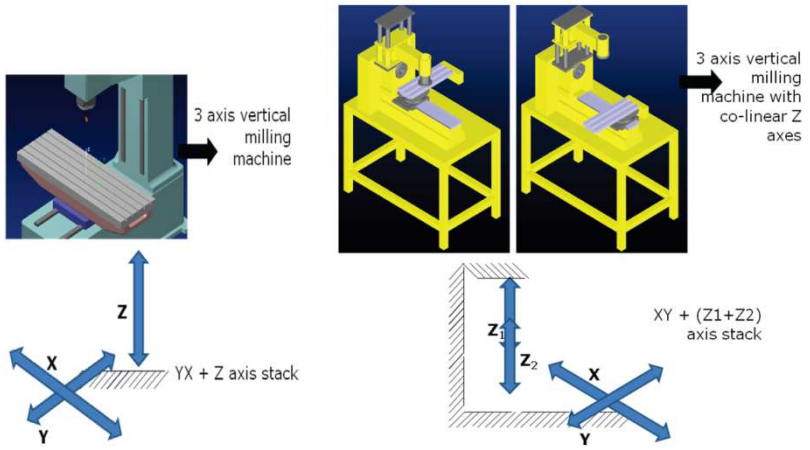

(a) (b)

Fig. 6. (a) $T_Z + T_Y T_X$ combination, (b) $(T_{Z1} + T_{Z2}) + T_X T_Y$ combination

For step 3 in the work window process flow, the analytical representation for Cases 1-7 is relatively simple, and related directly to the axis limits (all cases) and tool length (Cases 2, 3, 5 - 7). The complexity is introduced when coupling the kinematic chains for Cases 0, *R* and 0, *T*, and Cases 4, 5, and 6 with Cases 8-10. Reference planes need to be established to link the axes' grounds. Along with the axis stack order, the axes travel limits must be defined, as well as the revolve profiles, where appropriate. Set theory and Boolean operations are then performed to couple the fixture and tooling kinematic chains in relation to their bounding geometry.

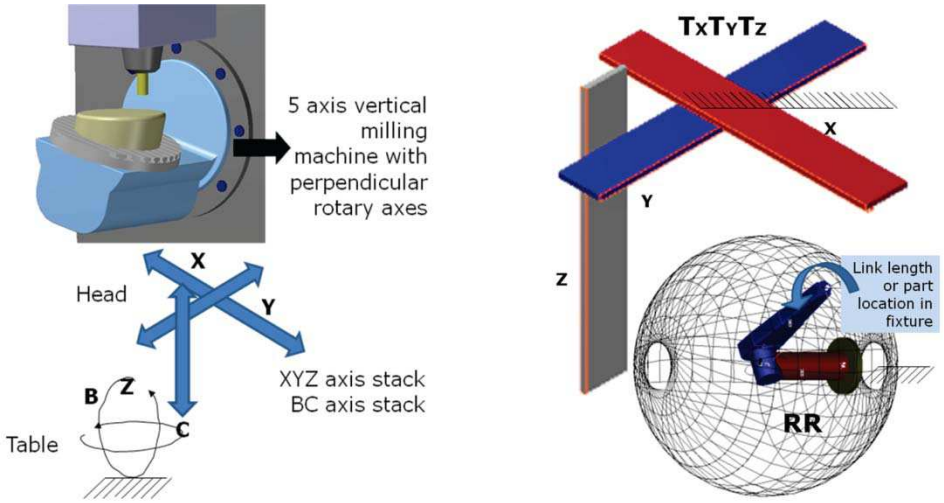

(a) (b)

Fig. 7. (a) 5 axis milling machine and basic structure, (b) RR+ $T_X T_Y T_Z$ combination

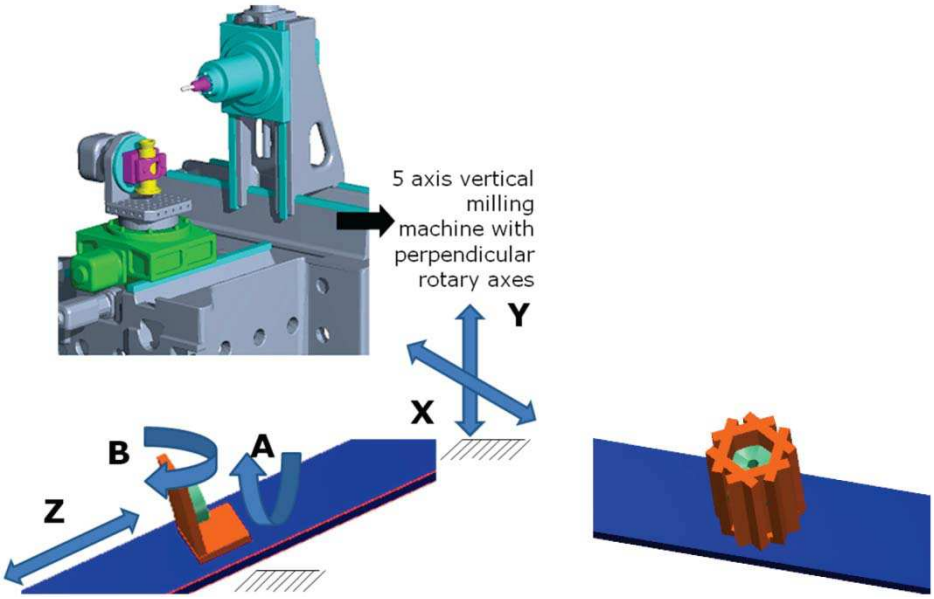

Fig. 8. 5 axis milling machine and basic structure, $T_Z R_B R_A + T_X T_Y$ combination, (b) revolve profile around the B axis at the home position (centre) of X axis

The addition of the rotary axes immediately reduces the maximum part size that can be machined. This reduction of available work space (or volumetric void) depends on the centre of rotation for the rotary axis, its rotational limits, and the axis stack; hence, the importance of being able to generate the revolve profile. The inclusion of the fixture(s) and part(s) modifies the rotary profile for an axis stack located on the table. For an axis stack located on the end-effector, the tool length (cutting tool or CMM probe) needs to be taken into consideration. This needs to be defined in order to assess the optimal fixture(s) positioning, the maximum part size or number of parts to be located on a fixture (i.e., a tombstone configuration consisting of multiple parts), the maximum tool length and width parameters, and the retraction travel path. The table based revolve profile must be contained or be a volumetric space subset within the workspace region defined by the *X, Y, Z* travel limits. For mechanisms that contain Cases 8 and 9, initial volumetric assessments need to be performed at the *X* and *Y* travel limits with the *Z* axis fully retracted while considering the tool offset to ensure no basic crash conditions and the maximum part/fixture conditions. Then assessments need to be performed at the rotary axes limits to determine orientation feasibilities. A sample of Boolean operations for the region defined by the tool offset (Figure 9 (a)) and then an axis stack on the *Z* axis (Figure 9 (b)) are illustrated in Figure 9.

2.2 Industrial robot solution approach

To start, the Denavit-Hartenberg notation (i.e., DH parameters) is presented to provide the background for the subsequent analyses, as the DH parameters are commonly used in the

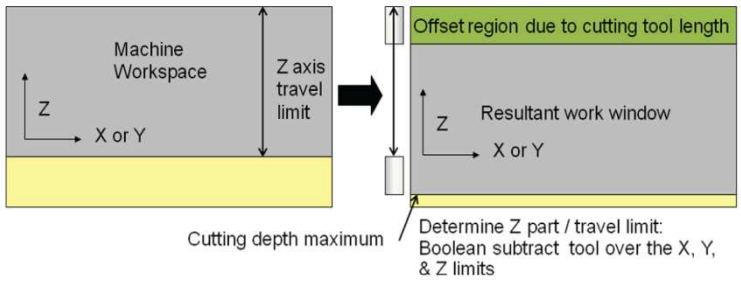

(a)

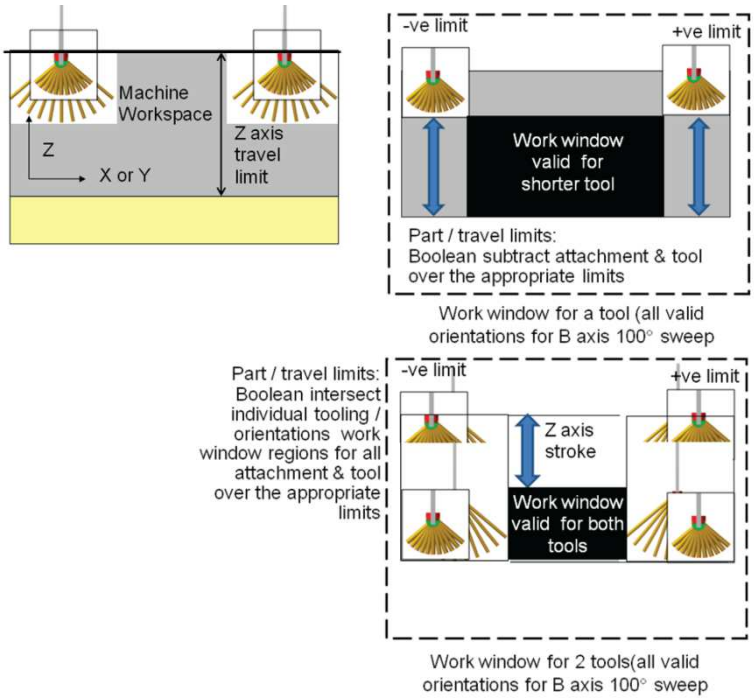

(b)

Fig. 9. Boolean operations for a Case 10 set of tools to establish valid operating region

robotics domain and provide a standard methodology to write the kinematic equations of a manipulator or end-effector. Each joint in a serial kinematic chain is assigned a coordinate frame. Using the DH notation (Denavit & Hartenberg , 1955), 4 parameters are needed to describe how a frame i relates to a previous frame $i-1$ as shown in Figure 10.

After assigning coordinate frames the four D-H parameters can be defined as following:

a_i - Link length is the distance along the common normal between the joint axes

α_i - Twist angle is the angle between the joint axes

θ_i - Joint angle is the angle between the links

d_i - Link offset is the displacement, along the joint axes between the links

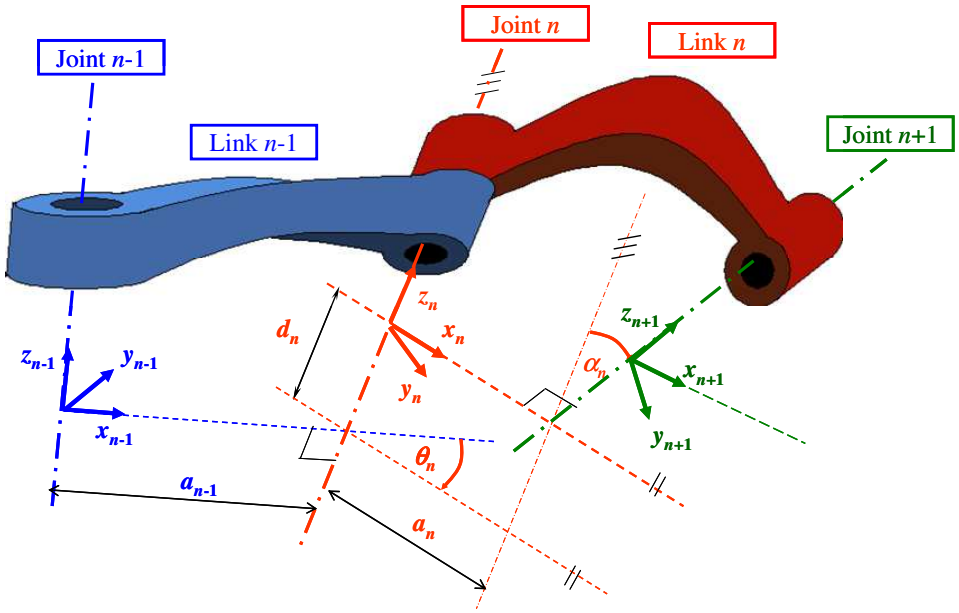

Fig. 10. Coordinate frames and D-H parameters

2.2.1 Empirical approach using a commercial robot simulation software package

The determination of open kinematic chain dexterity has been done using numerical and analytical methods. These methods are applied and compared using a six DOF manipulator, (Abdel-Malek & Yeh, 2000). The Jacobian formulation provides quantitative dexterity comparison between manipulators with different architectures. It was first applied to analyze serial robots and compared with parallel robots with the same DOF, (Pond & Carretro, 2011). Using the virtual angle analysis the dexterous workspace is generated to analyzed the orientation capability of a manipulator trough its equivalent mechanism (Dai & Shah, 2003). Placement of the manipulator has been done by implementing the Workspace towards the target points and subjecting it to a set of constraints to determine the reachability of the end-effector without using the inverse kinematics (Jingzhou Yang, et al., 2009).

Using the above information as a starting point, the methodology to generate the work window for robots using empirical equations follows. Two robots were selected with different kinematic structures (an ABB IRB 140 Robot and a Fanuc M16) and their work window was generated using the Workspace 5 robotic simulation software. A systematic manual valid point generation approach is used to develop the algorithm that supports both procedures. After this was completed, analytical equations were developed empirically and tested for their validity using different examples, an approach conceptually similar to that taken by Abdel-Malek & Yeh (2000). Then the methodology was expanded upon to reflect the problem being solved. By varying joint values to get the complete space representation with the desired orientation (in this example, the orientation is 'normal to the robot base' as this represents common pick and place operations associated with material handling), only four joints are used: Joint 1, Joint 2, Joint 3, and Joint 5. Joint 4 and Joint 6 remain constant. For this study the detailed kinematic information for the ABB IRB 140 Robot and Fanuc M16

robots is presented below. The ABB IRB 140 kinematic structure diagram is shown in Figure 11 and its D-H parameters are given in Table 2.

i	d_i	θ_i	a_i	α_i
1	d_1	$\theta_1 = 0^\circ$	a_1	-90°
2	0	$\theta_2 = -90^\circ$	a_2	0°
3	0	$\theta_3 = 180^\circ$	0	90°
4	d_4	$\theta_4 = 0^\circ$	0	-90°
5	0	$\theta_5 = 0^\circ$	0	90°
6	d_6	$\theta_6 = -90^\circ$	0	90°

Table 2. D-H parameters for the ABB IRB 140 Robot

The Fanuc M16 kinematic structure diagram is shown in Figure 12 and its D-H parameters are given in Table 3.

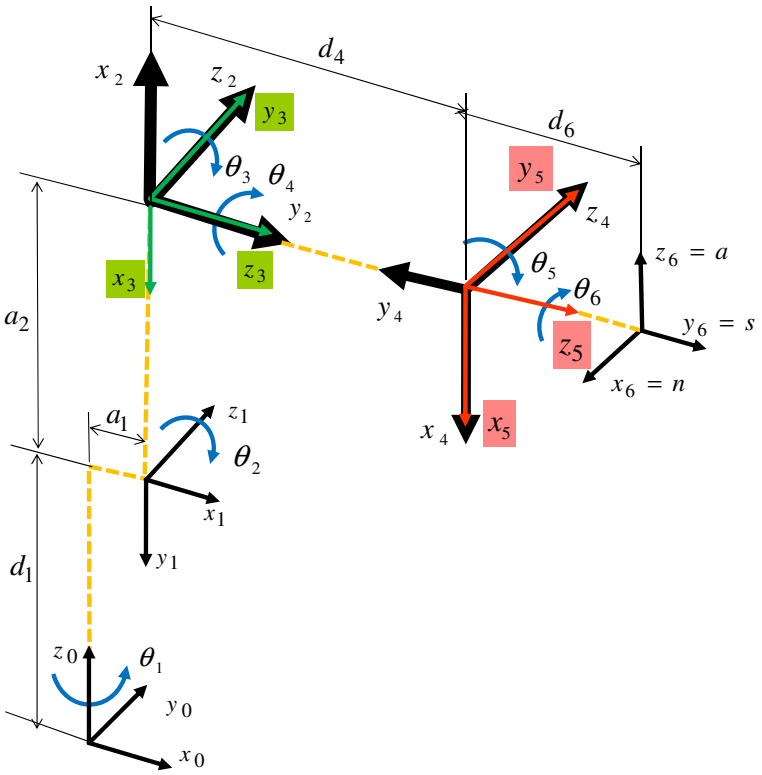

Fig. 11. Kinematic structure of the ABB IRB 140 robot

i	d_i	θ_i	a_i	α_i
1	d_1	$\theta_1 = 0^\circ$	a_1	–90°
2	0	$\theta_2 = -90^\circ$	a_2	180°
3	0	$\theta_3 = 180^\circ$	a_3	90°
4	d_4	$\theta_4 = 0^\circ$	0	–90°
5	0	$\theta_5 = 0^\circ$	0	90°
6	d_6	$\theta_6 = 180^\circ$	0	180°

Table 3. D-H parameters for the Fanuc M16 Robot

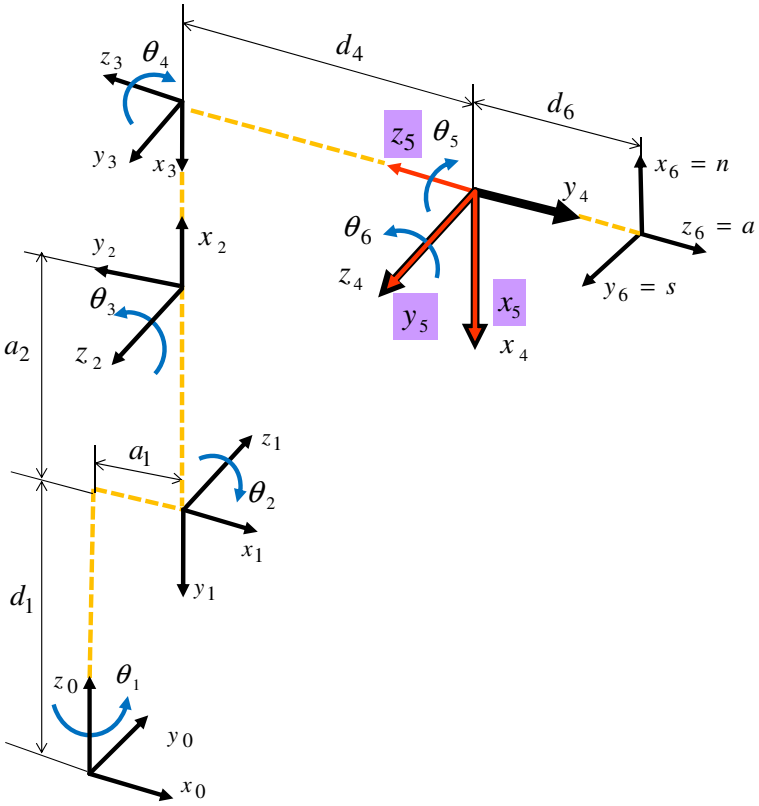

Fig. 12. Kinematic structure of the Fanuc M16 Robot

Using a commercial simulation and off-line programming software Workspace 5, the work window (subspace with 'normal to the base' orientation) is generated for the ABB IRB 140 robot. The black net represents the 2D workspace and the green coordinate frames represent

the work window region. The 2D set of points for the ABB IRB 140 is presented in Figure 13. Similarly, the work window (subspace with 'normal to the base' orientation) is generated for the Fanuc M16 robot and this set of 2D points is presented in Figure 14.

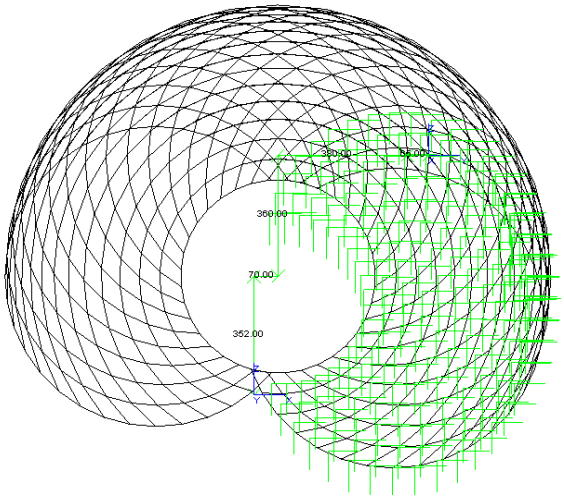

Fig. 13. Work window for the ABB IRB 140 Robot for the 90 degree (normal) orientation

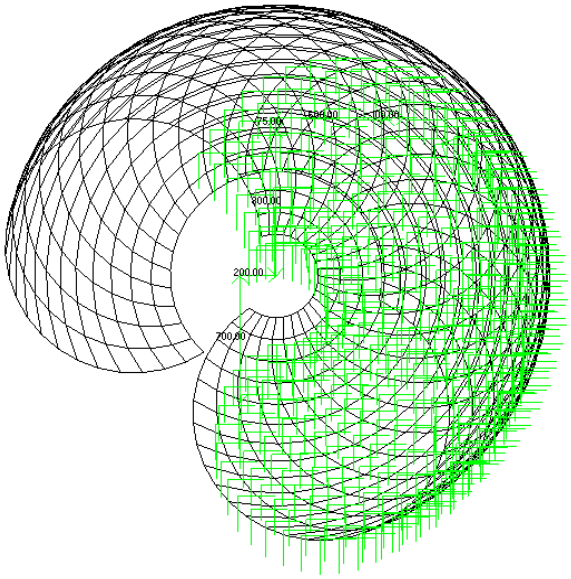

Fig. 14. Work window for the Fanuc M16 Robot for 90 degree (normal) orientation

Upon combining the procedures for the generation both work windows, an empirical formula for the joint five angle is developed, which is shown in equation (1).

$$\theta_5 = K\phi - (\theta_2 + K\theta_3) \tag{1}$$

The parameter K in Equation 1 is calculated using the formula below:

$$K = \cos\alpha_2 \tag{2}$$

Where α_2 is the Joint 2 twist angle.

The generalized algorithm for generating the work window for two different kinematic structures is given in Figure 15. This solution is valid for 6 DOF robots with rotational joints and the Fanuc and ABB robot kinematic structures. The outcome of the algorithm is either a 2D or 3D work window.

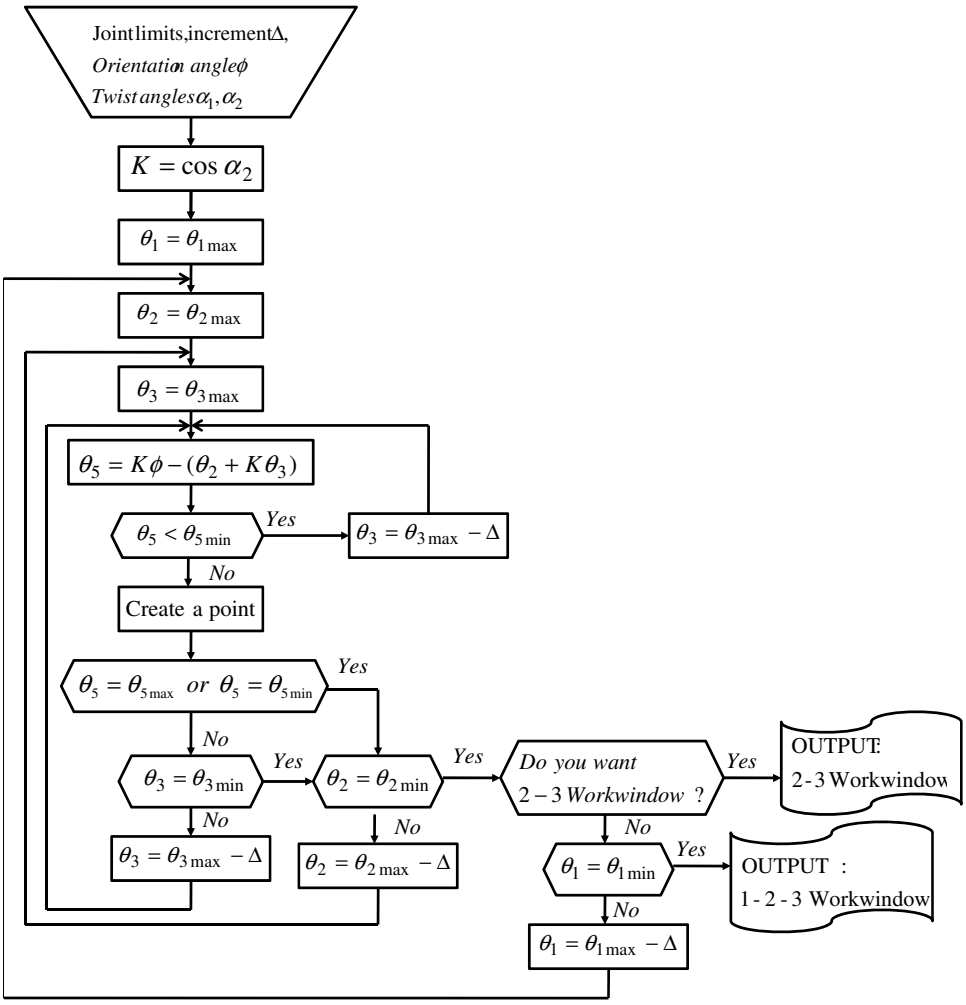

Fig. 15. Algorithm for work window generation

2.2.2 Generation of Work window using analytical equations

In the kinematic analysis of the manipulator position, there are two separate problems to be solved: the direct kinematics, and inverse kinematics. Assessing the direct kinematics involves solving the forward transformation equation to find the location of the hand in terms of the angles and displacements between the links. The angles and displacements between the links are called joint coordinates and are described with link variables, while the location of the hand in space is described using Cartesian coordinates. Inverse kinematics involves solving the inverse transformation equation to find the relationships between the links of the manipulator from the location of the hand in space. A serial link manipulator is a series of links, which connects the end-effector to the base, with each link connected to the next by an actuated joint. If a coordinate frame is attached to each link, the relationship between two links can be described with a homogeneous transformation matrix using D-H rules (Denavit & Hartenberg, 1955), and they are named ${}^{i-1}A_i$, where i is number of joints.

$$ {}^{i-1}A_i = \begin{bmatrix} \cos\theta_i & -\cos\alpha_i \sin\theta_i & \sin\alpha_i \sin\theta_i & a_i \cos\theta_i \\ \sin\theta_i & \cos\alpha_i \cos\theta_i & -\sin\alpha_i \cos\theta_i & a_i \sin\theta_i \\ 0 & \sin\alpha_i & \cos\alpha_i & d_i \\ 0 & 0 & 0 & 1 \end{bmatrix} \tag{3} $$

The robot can now be kinematically modeled by using the link transforms:

$$ {}^0A_n = {}^0A_1 {}^1A_2 {}^2A_3 \cdots {}^{i-1}A_i \cdots {}^{n-1}A_n \tag{4} $$

Where ${}^0A_n$ is the pose of the end-effector relative to base; ${}^{i-1}A_i$ is the link transform for the i^{th} joint; and n is the number of links.

For the ABB IRB 140 robot, six homogeneous transformation matrices have been developed using Maple 12 symbolic manipulation software, Equation 2 and the D-H parameters from Table 2.

$$ {}^0A_1 = \begin{bmatrix} \cos\theta_1 & -\cos\alpha_1 \sin\theta_1 & \sin\alpha_1 \sin\theta_1 & a_1 \cos\theta_1 \\ \sin\theta_1 & \cos\alpha_1 \cos\theta_1 & -\sin\alpha_1 \cos\theta_1 & a_1 \sin\theta_1 \\ 0 & \sin\alpha_1 & \cos\alpha_1 & d_1 \\ 0 & 0 & 0 & 1 \end{bmatrix} = \begin{bmatrix} \cos\theta_1 & 0 & -\sin\theta_1 & a_1 \cos\theta_1 \\ \sin\theta_1 & 0 & \cos\theta_1 & a_1 \sin\theta_1 \\ 0 & -1 & 0 & d_1 \\ 0 & 0 & 0 & 1 \end{bmatrix} \tag{5} $$

$$ {}^1A_2 = \begin{bmatrix} \cos\theta_2 & -\cos\alpha_2 \sin\theta_2 & \sin\alpha_2 \sin\theta_2 & a_2 \cos\theta_2 \\ \sin\theta_2 & \cos\alpha_2 \cos\theta_2 & -\sin\alpha_2 \cos\theta_2 & a_2 \sin\theta_2 \\ 0 & \sin\alpha_2 & \cos\alpha_2 & d_2 \\ 0 & 0 & 0 & 1 \end{bmatrix} = \begin{bmatrix} \cos\theta_2 & -\sin\theta_2 & 0 & a_2 \cos\theta_2 \\ \sin\theta_2 & \cos\theta_2 & 0 & a_2 \sin\theta_2 \\ 0 & 0 & 1 & 0 \\ 0 & 0 & 0 & 1 \end{bmatrix} \tag{6} $$

$$ {}^{2}A_{3} = \begin{bmatrix} \cos\theta_3 & -\cos\alpha_3\sin\theta_3 & \sin\alpha_3\sin\theta_3 & a_3\cos\theta_3 \\ \sin\theta_3 & \cos\alpha_3\cos\theta_3 & -\sin\alpha_3\cos\theta_3 & a_3\sin\theta_3 \\ 0 & \sin\alpha_3 & \cos\alpha_3 & d_3 \\ 0 & 0 & 0 & 1 \end{bmatrix} = \begin{bmatrix} \cos\theta_3 & 0 & \sin\theta_3 & 0 \\ \sin\theta_3 & 0 & -\cos\theta_3 & 0 \\ 0 & 1 & 0 & 0 \\ 0 & 0 & 0 & 1 \end{bmatrix} \quad (7) $$

$$ {}^{3}A_{4} = \begin{bmatrix} \cos\theta_4 & -\cos\alpha_4\sin\theta_4 & \sin\alpha_4\sin\theta_4 & a_4\cos\theta_4 \\ \sin\theta_4 & \cos\alpha_4\cos\theta_4 & -\sin\alpha_4\cos\theta_4 & a_4\sin\theta_4 \\ 0 & \sin\alpha_4 & \cos\alpha_4 & d_4 \\ 0 & 0 & 0 & 1 \end{bmatrix} = \begin{bmatrix} \cos\theta_4 & 0 & -\sin\theta_4 & 0 \\ \sin\theta_4 & 0 & \cos\theta_4 & 0 \\ 0 & -1 & 0 & d_4 \\ 0 & 0 & 0 & 1 \end{bmatrix} \quad (8) $$

$$ {}^{4}A_{5} = \begin{bmatrix} \cos\theta_5 & -\cos\alpha_5\sin\theta_5 & \sin\alpha_5\sin\theta_5 & a_5\cos\theta_5 \\ \sin\theta_5 & \cos\alpha_5\cos\theta_5 & -\sin\alpha_5\cos\theta_5 & a_5\sin\theta_5 \\ 0 & \sin\alpha_5 & \cos\alpha_5 & d_5 \\ 0 & 0 & 0 & 1 \end{bmatrix} = \begin{bmatrix} \cos\theta_5 & 0 & \sin\theta_5 & 0 \\ \sin\theta_5 & 0 & -\cos\theta_5 & 0 \\ 0 & 1 & 0 & 0 \\ 0 & 0 & 0 & 1 \end{bmatrix} \quad (9) $$

$$ {}^{5}A_{6} = \begin{bmatrix} \cos\theta_6 & -\cos\alpha_6\sin\theta_6 & \sin\alpha_6\sin\theta_6 & a_6\cos\theta_6 \\ \sin\theta_6 & \cos\alpha_6\cos\theta_6 & -\sin\alpha_6\cos\theta_6 & a_6\sin\theta_6 \\ 0 & \sin\alpha_6 & \cos\alpha_6 & d_6 \\ 0 & 0 & 0 & 1 \end{bmatrix} = \begin{bmatrix} \cos\theta_6 & 0 & \sin\theta_6 & 0 \\ \sin\theta_6 & 0 & -\cos\theta_6 & 0 \\ 0 & 1 & 0 & d_6 \\ 0 & 0 & 0 & 1 \end{bmatrix} \quad (10) $$

The ABB IRB 140 robot can now be kinematically modeled by using Equations 4-10.

$$ {}^{0}A_{6} = {}^{0}A_{1}\,{}^{1}A_{2}\,{}^{2}A_{3}\,{}^{3}A_{4}\,{}^{4}A_{5}\,{}^{5}A_{6} \quad (11) $$

The pose matrix of the end-effector relative to the base is presented in Equation 12.

$$ {}^{0}A_{6} = \begin{bmatrix} n_x & s_x & a_x & p_x \\ n_y & s_y & a_y & p_y \\ n_z & s_z & a_z & p_z \\ 0 & 0 & 0 & 1 \end{bmatrix} \quad (12) $$

The end-effector orientation is defined with the rotation matrix. The upper $3X3$ sub matrices of the homogeneous transformation matrices Equation 11, represents the rotational matrix, Equation 13. The graphical representation of the end-effector is shown in Figure16.

$$ {}^{0}R_{6} = \begin{bmatrix} n_x & s_x & a_x \\ n_y & s_y & a_y \\ n_z & s_z & a_z \end{bmatrix} \quad (13) $$

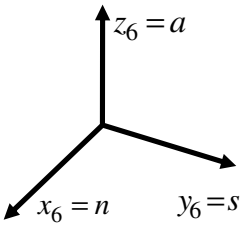

Fig. 16. The end-effector frame of the ABB IRB 140 robot

The normal vector n is along x_6 axis, the sliding vector s is along y_6 axis, and the approach vector a is along z_6 axis. The orientation of the end-effector, relative to the robot base frame, is defined with the three vectors: n, s, and a. Their projections onto the robot base frame are given with the rotational matrix ${}^0R_6$. For the ABB IRB 140 Robot the relation between end-effector and base frame, when the end-effector is normal to the robot base, is graphically shown in Figure 17. The orientation matrix for the given position is calculated (see Equation 13).

$$ {}^0R_6 = \begin{bmatrix} 0 & 0 & 1 \\ -1 & 0 & 0 \\ 0 & -1 & 0 \end{bmatrix} \tag{14} $$

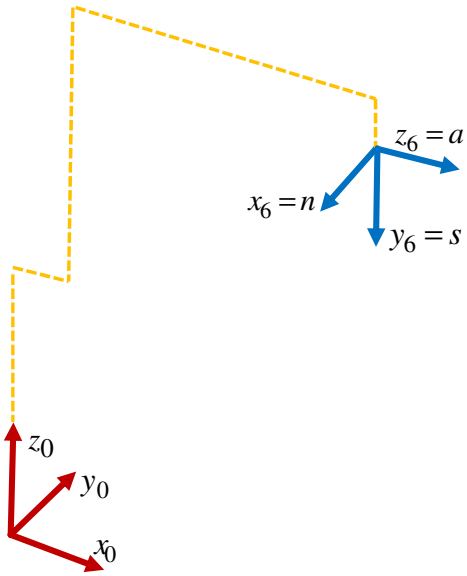

Fig. 17. The end-effector frame of the ABB IRB 140 robot

The calculation of the 2D end-effector orientation is dependent on the three joint angles: Joint 2, Joint 3 and Joint 5. The formula for Joint 5 is generated by assigning initial values for the Joint 1, Joint 4 and Joint 6 in the forward kinematic solution. The rotational matrix in that case is calculated and is shown in Equation 15.

$$ {}^{0}R_{6} = \begin{bmatrix} 0 & \cos(\theta_2+\theta_3)\sin\theta_5+\sin(\theta_2+\theta_3)\cos\theta_5 & -\cos(\theta_2+\theta_3)\cos\theta_5+\sin(\theta_2+\theta_3)\sin\theta_5 \\ -1 & 0 & 0 \\ 0 & -\sin(\theta_2+\theta_3)\sin\theta_5+\cos(\theta_2+\theta_3)\cos\theta_5 & \cos(\theta_2+\theta_3)\sin\theta_5+\sin(\theta_2+\theta_3)\cos\theta_5 \end{bmatrix} \quad (15) $$

By combining Equation 14 and 15 the formula for the Joint 5 angle is generated.

$$ \theta_5 = a\tan 2\left(\frac{\sin(\theta_2+\theta_3)}{-\cos(\theta_2+\theta_3)}\right) \quad (16) $$

To be able to generate complete work window, the Joint 2 and Joint 3 angles must vary between their given limits for the desired increment value Δ and using the forward kinematic solution to generate the solution for Joint 5.
Equation 16 was evaluated using the commercial software Matlab. The results were compared to the forward kinematics calculated using the Maple 12 software and the Workspace 5 simulation and off-line programming software (Figure 18).

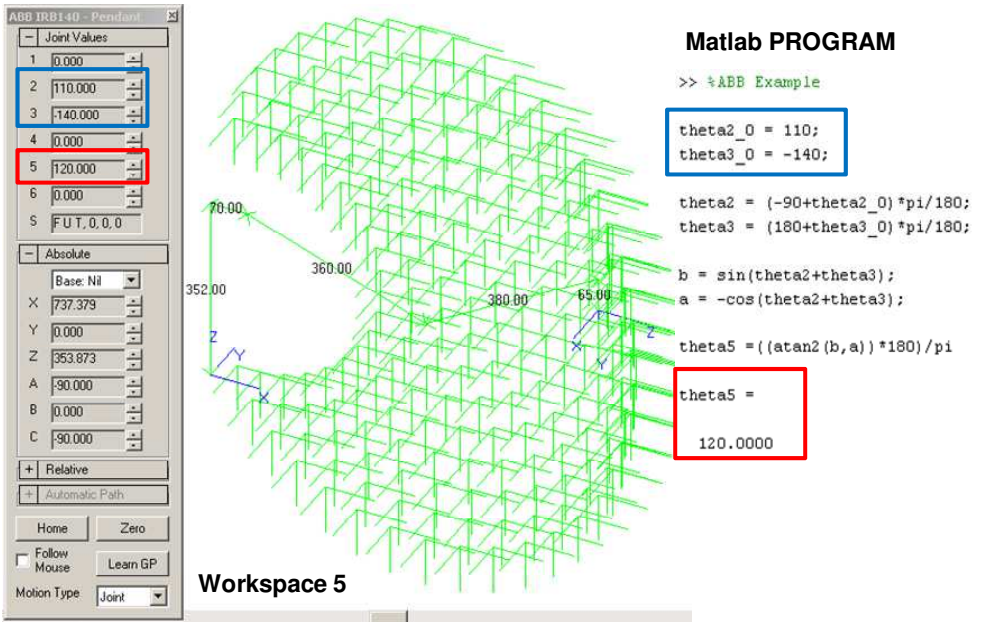

Fig. 18. Evaluation of the formula for the ABB IRB 140 robot

The forward kinematic calculations for the Fanuc M16 robot are done using Equations 2 and 3 and Table 3, which are shown in equations 17-22.

$$ {}^{0}A_{1} = \begin{bmatrix} \cos\theta_1 & -\cos\alpha_1 \sin\theta_1 & \sin\alpha_1 \sin\theta_1 & a_1 \cos\theta_1 \\ \sin\theta_1 & \cos\alpha_1 \cos\theta_1 & -\sin\alpha_1 \cos\theta_1 & a_1 \sin\theta_1 \\ 0 & \sin\alpha_1 & \cos\alpha_1 & d_1 \\ 0 & 0 & 0 & 1 \end{bmatrix} = \begin{bmatrix} \cos\theta_1 & 0 & -\sin\theta_1 & a_1 \cos\theta_1 \\ \sin\theta_1 & 0 & \cos\theta_1 & a_1 \sin\theta_1 \\ 0 & -1 & 0 & d_1 \\ 0 & 0 & 0 & 1 \end{bmatrix} \quad (17) $$

$$ {}^{1}A_{2} = \begin{bmatrix} \cos\theta_2 & -\cos\alpha_2 \sin\theta_2 & \sin\alpha_2 \sin\theta_2 & a_2 \cos\theta_2 \\ \sin\theta_2 & \cos\alpha_2 \cos\theta_2 & -\sin\alpha_2 \cos\theta_2 & a_2 \sin\theta_2 \\ 0 & \sin\alpha_2 & \cos\alpha_2 & d_2 \\ 0 & 0 & 0 & 1 \end{bmatrix} = \begin{bmatrix} \cos\theta_2 & \sin\theta_2 & 0 & a_2 \cos\theta_2 \\ \sin\theta_2 & -\cos\theta_2 & 0 & a_2 \sin\theta_2 \\ 0 & 0 & -1 & 0 \\ 0 & 0 & 0 & 1 \end{bmatrix} \quad (18) $$

$$ {}^{2}A_{3} = \begin{bmatrix} \cos\theta_3 & -\cos\alpha_3 \sin\theta_3 & \sin\alpha_3 \sin\theta_3 & a_3 \cos\theta_3 \\ \sin\theta_3 & \cos\alpha_3 \cos\theta_3 & -\sin\alpha_3 \cos\theta_3 & a_3 \sin\theta_3 \\ 0 & \sin\alpha_3 & \cos\alpha_3 & d_3 \\ 0 & 0 & 0 & 1 \end{bmatrix} = \begin{bmatrix} \cos\theta_3 & 0 & \sin\theta_3 & a_3 \cos\theta_3 \\ \sin\theta_3 & 0 & -\cos\theta_3 & a_3 \sin\theta_3 \\ 0 & 1 & 0 & 0 \\ 0 & 0 & 0 & 1 \end{bmatrix} \quad (19) $$

$$ {}^{3}A_{4} = \begin{bmatrix} \cos\theta_4 & -\cos\alpha_4 \sin\theta_4 & \sin\alpha_4 \sin\theta_4 & a_4 \cos\theta_4 \\ \sin\theta_4 & \cos\alpha_4 \cos\theta_4 & -\sin\alpha_4 \cos\theta_4 & a_4 \sin\theta_4 \\ 0 & \sin\alpha_4 & \cos\alpha_4 & d_4 \\ 0 & 0 & 0 & 1 \end{bmatrix} = \begin{bmatrix} \cos\theta_4 & 0 & -\sin\theta_4 & 0 \\ \sin\theta_4 & 0 & \cos\theta_4 & 0 \\ 0 & -1 & 0 & d_4 \\ 0 & 0 & 0 & 1 \end{bmatrix} \quad (20) $$

$$ {}^{4}A_{5} = \begin{bmatrix} \cos\theta_5 & -\cos\alpha_5 \sin\theta_5 & \sin\alpha_5 \sin\theta_5 & a_5 \cos\theta_5 \\ \sin\theta_5 & \cos\alpha_5 \cos\theta_5 & -\sin\alpha_5 \cos\theta_5 & a_5 \sin\theta_5 \\ 0 & \sin\alpha_5 & \cos\alpha_5 & d_5 \\ 0 & 0 & 0 & 1 \end{bmatrix} = \begin{bmatrix} \cos\theta_5 & 0 & \sin\theta_5 & 0 \\ \sin\theta_5 & 0 & -\cos\theta_5 & 0 \\ 0 & 1 & 0 & 0 \\ 0 & 0 & 0 & 1 \end{bmatrix} \quad (21) $$

$$ {}^{5}A_{6} = \begin{bmatrix} \cos\theta_6 & -\cos\alpha_6 \sin\theta_6 & \sin\alpha_6 \sin\theta_6 & a_6 \cos\theta_6 \\ \sin\theta_6 & \cos\alpha_6 \cos\theta_6 & -\sin\alpha_6 \cos\theta_6 & a_6 \sin\theta_6 \\ 0 & \sin\alpha_6 & \cos\alpha_6 & d_6 \\ 0 & 0 & 0 & 1 \end{bmatrix} = \begin{bmatrix} \cos\theta_6 & \sin\theta_6 & 0 & 0 \\ \sin\theta_6 & -\cos\theta_6 & 0 & 0 \\ 0 & 0 & -1 & d_6 \\ 0 & 0 & 0 & 1 \end{bmatrix} \quad (22) $$

Similarly to the previous calculations, the end-effector orientation matrix is found. The graphical representation of the end-effector is shown in Figure 19.

For the Fanuc M16 Robot the relationship between end-effector and base frame, when end-effector is normal to the robot base, is graphically shown in Figure 20. The orientation matrix for the given position is calculated using Equation 23.

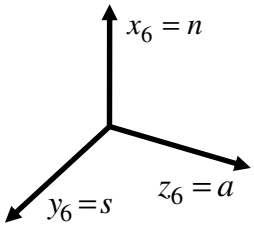

Fig. 19. The end-effector frame of the Fanuc M16 robot

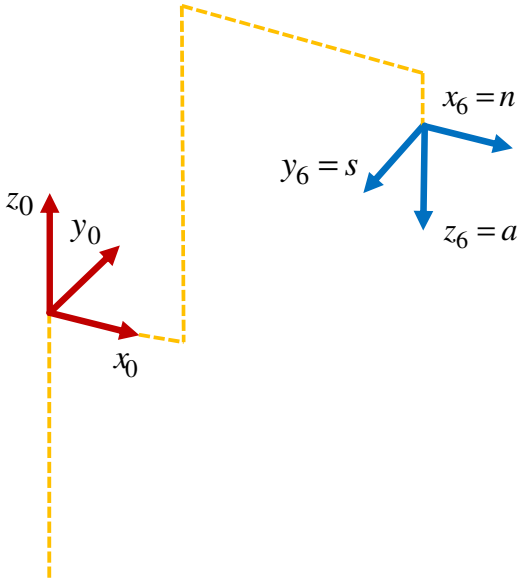

Fig. 20. The end-effector frame of the Fanuc M16 robot

$$ {}^{0}R_{6} = \begin{bmatrix} 1 & 0 & 0 \\ 0 & -1 & 0 \\ 0 & 0 & -1 \end{bmatrix} \tag{23} $$

The rotational matrix in this case is calculated and is shown in Equation 24.

$$ {}^{0}R_{6} = \begin{bmatrix} -\cos(\theta_2 - \theta_3)\cos\theta_5 - \sin(\theta_2 - \theta_3)\sin\theta_5 & 0 & -\cos(\theta_2 - \theta_3)\sin\theta_5 + \sin(\theta_2 - \theta_3)\cos\theta_5 \\ 0 & -1 & 0 \\ -\cos(\theta_2 - \theta_3)\sin\theta_5 + \sin(\theta_2 - \theta_3)\cos\theta_5 & 0 & \sin(\theta_2 - \theta_3)\sin\theta_5 + \cos(\theta_2 - \theta_3)\cos\theta_5 \end{bmatrix} \tag{24} $$

By combining Equations 23 and 24, the formula for Joint 5 angle is generated.

$$\theta_5 = a\tan 2\left(\frac{-\sin(\theta_2 - \theta_3)}{-\cos(\theta_2 - \theta_3)}\right) \tag{25}$$

To be able to generate the complete work window, again the Joint 2 and Joint 3 angles must be varied between their given limits for the desired increment value Δ and using the forward kinematic solution to generate the solution for the Joint 5.
As with the ABB IRB 140 robot, this resulting equation 25 is evaluated using Matlab, and compared with result assessments Maple 12 and Workspace 5 (Figure 21).

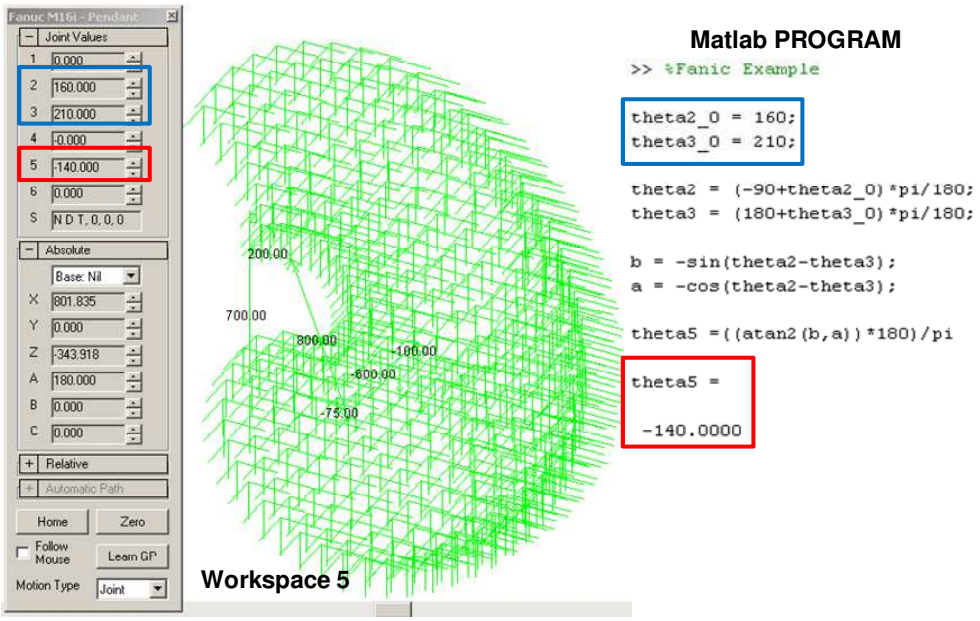

Fig. 21. Evaluation of the formula for Fanuc M16 Robot

Equations 16 and 25 can be unified into one general formula for calculating Joint 5 angle for either ABB IRB 140 robot or Fanuc M16 robot by using the parameter K in Equation 2. The unified formula is presented in Equation 26.

$$\theta_5 = a\tan 2\left(\frac{K\sin(\theta_2 + K\theta_3)}{-\cos(\theta_2 + K\theta_3)}\right) \tag{26}$$

This methodology can be applied to any similar kinematic structure and the unification procedure can be extended. The formula is valid for any desired orientation. The example using a 45 degree orientation for the ABB IRB 140 robot is illustrated in Figures 22 and 23. As with the machine tool example illustrated in Figure 9 (b), the Boolean intersection of the selected 45° orientation and the 90 ° normal to the base regions is the zone where both orientations are valid (Figure 23), and where the part should be located if both orientations are required for the process travel paths.

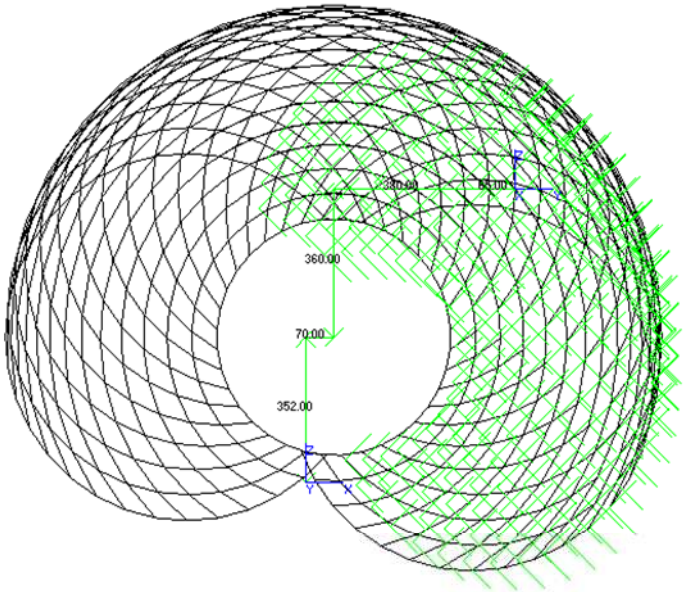

Fig. 22. Work window for the ABB IRB 140 robot for the 45 degree orientation

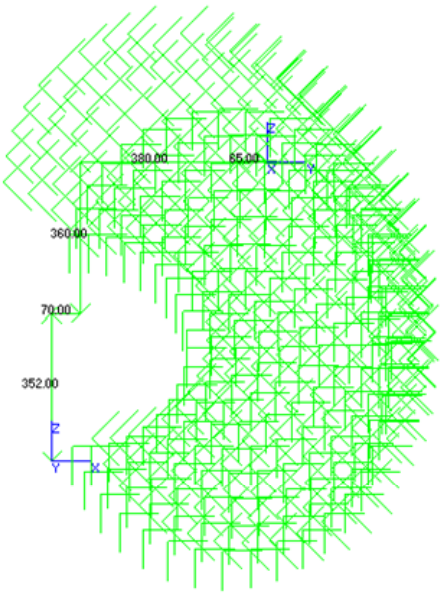

Fig. 23. Work window for the ABB IRB 140 robot showing the comparison between the 90 normal to the base orientation and the 45 degree orientation

To facilitate the 6 DOF work window calculation, empirical and analytical methods are used and validated. From the empirical study, it found out that Joint 2, Joint 3, and Joint 5 play the most important role. By varying Joint 2 and Joint 3 between their limits, Joint 5 needs to be calculated to satisfy the desired end-effector orientation angle. The study of a repeatable procedure led to the generation of the analytical method.
Two kinematically different robots are selected and their work windows are generated: the ABB IRB 140 and Fanuc M16 robots. The resulting work window space can then be assessed using Boolean operations to determine the valid working zone for multiple travel paths, orientations, or regions of overlap for a manufacturing cell. This is illustrated for the 90 degree normal to the base and selected 45 degree orientation example.

3. Robot cell case study

For the selected example, the work window is generated using the empirical formula (algorithm in Figure 11) and evaluated with analytical solution (Figure 24). Three 6DOF ABB robots are place in a work cell. The desired orientation is required for synchronous motion. The robots' placement will depend on the end-effector orientation. Using the work window for each robot, the layout can be done quickly, accurately and options can then be assessed. For example, the consideration that the robots may offset and sliding rails (or a 7th axis) added such that one robot could be repositioned to perform the other robot's tasks if a robot is non-performing for a reason. Reduced productivity would result, but production could still continue.

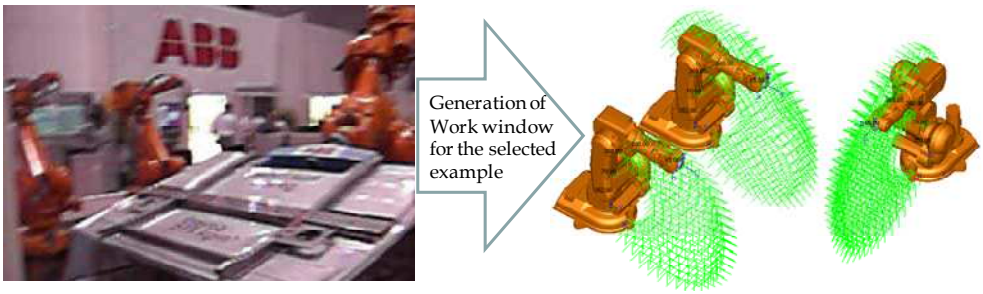

Fig. 24. Work window for the selected example

4. Conclusion

To conclude, a methodology to predetermine regions of feasible operation for multiple kinematic chain mechanisms and manufacturing cells is presented. The approach differs for mechanisms consisting of 1, 2, and 3 DOF subsets linked together via reference frames, and 6 DOF industrial robots. However, after the basic region of valid operation is determined, assessment of the part location and travel paths can be performed. With complex system configurations, it is not intuitive to define the region of task feasibility for the initial design and as well as design alternatives, as there is much coupling related to the kinematic structures and their manipulability, tooling, fixtures, part geometry and task requirements. Changing an operation / task set or a system reconfiguration can be

executed virtually, and these methods employed to determine feasibility prior to physical set ups or modification in the manufacturing environment, which represents a time and cost savings.

5. References

Abdel-Malek, K. & Yeh, H. J. (2000). Local Dexterity Analysis for Open Kinematic Chains, *Mechanism and Machine Theory*, Vol. 35, pp. 131-154.

Anonymous - Okuma, 2002, Okuma Twin Star LT Series Turning Centres with Twin Spindles, *LT Series - (1) –300*, Okuma Co.

Castelli, G.; Ottaviano, E. & Ceccarelli, M. (2008). A Fairly General Algorithm to Evaluate Workspace Characteristics of Serial and Parallel Manipulators, *Mechanics Based Design of Structures and Machines*, Vol. 36, pp. 14-33

Cebula, A.J. & Zsombor-Murray, P.J. (2006). Formulation of the Workspace Equation for Wrist-Partitioned Spatial Manipulators, *Mechanisms and Machine Theory*, Vol 41, pp. 778-789

Ceccarelli, M. & Lanni, C. (2003). A Multi-objective Optimum Design of General 3R Manipulators for Prescribed Workspace Limits, *Mechanisms and Machine Theory*, Vol. 39, pp. 119-132

Ceccarelli, M. & Vinciguerra, A. (1995). On the Workspace of the General 4R Manipulators, *The International Journal of Robotics Research*, Vol.14, pp.152-160

Ceccarelli, M. (1996). A Formulation for the Workspace Boundary of General N-revolute Manipulators, *Mechanisms and Machine Theory*, Vol. 31, pp. 637-646

Dai, J. & Shah, P. (2003). Orientation Capability Planar Manipulators Using Virtual Joint Angle Analysis, *Mechanism and Machine Theory*, Vol. 38, pp. 241-252

Denavit J. & Hartenberg R. S. (1955). A Kinematic Notation for Lower-pair Mechanisms Based on Matrices, *Journal of Applied Mechanics,* Vol. 77, pp. 215-221.

Djuric, A. & Urbanic, R. J. (2009). A Methodology for Defining the Functional Space (Work Window) for a Machine Configuration, *3nd International Conference on Changeable, Agile, Reconfigurable and Virtual Production*, CD-ROM, Munich, October 5th-7th, 2009

Djuric, A. M. & ElMaraghy, W. H. (2008). Filtering Boundary Points of the Robot Workspace, *5th International Conference on Digital Enterprise Technology*. Nantes, France, October 2008

ElMaraghy, H. A. & ElMaraghy, W. H. (1993). Bridging the Gap Between Process Planning and Production Planning and Control, *CIRP Journal of Manufacturing Systems*, Vol. 22, No. 1, pp. 5-11

ElMaraghy, H. A. (2005). Flexible and Reconfigurable Manufacturing Systems Paradigms, *International Journal of Flexible Manufacturing Systems, Special Issue on Reconfigurable Manufacturing Systems,* Vol. 17, pp. 261-276

ElMaraghy, H. A. (2008). *Changeable and Reconfigurable Manufacturing Systems,* (editor) Springer-Verlag (Publisher), ISBN: 978-1-84882-066-1

Hedrick R. & Urbanic, R. J. (2007). A Methodology for Managing Change when Reconfiguring a Manufacturing System, *2nd International Conference on Changeable, Agile, Virtual and Reconfigurable Production (CARV),* pp. 992-1001

Koren, Y.; Heisel, U.; Jovane, F.; Moriwaki, T.; Pritchow, G.; Van Brussel, H. & Ulsoy, A.G. (1999). Reconfigurable Manufacturing Systems, *CIRP Annals*, Vol. 48, No. 2.

Nof, S.Y. (1999). *Handbook of Industrial Robotics*, 2nd edn. New York: John Wiley & Sons.

Pond, G. & Carretro, J. (2011). Dexterity Measures and Their Use in Quantitative Dexterity Comparisons, *Meccanica*, Vol. 46, pp. 51-64

Yang, J.; Yu, W.; Kim, J. & Abdel-Malet, K. (2009). On the Placement of Open-Loop Robotic Manipulators for Reachability, *Mechanism and Machine Theory*, Vol. 44, pp. 671-684

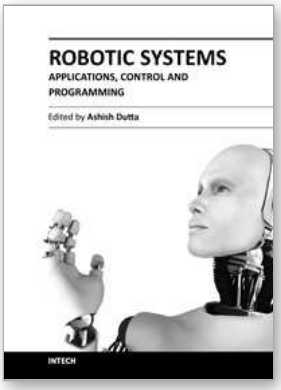

Robotic Systems - Applications, Control and Programming
Edited by Dr. Ashish Dutta

ISBN 978-953-307-941-7
Hard cover, 628 pages
Publisher InTech
Published online 03, February, 2012
Published in print edition February, 2012

This book brings together some of the latest research in robot applications, control, modeling, sensors and algorithms. Consisting of three main sections, the first section of the book has a focus on robotic surgery, rehabilitation, self-assembly, while the second section offers an insight into the area of control with discussions on exoskeleton control and robot learning among others. The third section is on vision and ultrasonic sensors which is followed by a series of chapters which include a focus on the programming of intelligent service robots and systems adaptations.

InTech Europe
University Campus STeP Ri
Slavka Krautzeka 83/A
51000 Rijeka, Croatia
Phone: +385 (51) 770 447
Fax: +385 (51) 686 166
www.intechopen.com

InTech China
Unit 405, Office Block, Hotel Equatorial Shanghai
No.65, Yan An Road (West), Shanghai, 200040, China
中国上海市延安西路65号上海国际贵都大饭店办公楼405单元
Phone: +86-21-62489820
Fax: +86-21-62489821